Beryl as an indicator for elemental behavior during magmatic evolution and metasomatism in the large Shihuiyao Rb-Nb-Ta-Be deposit, Inner Mongolia, NE China

Zhenpeng Duan, Shao-Yong Jiang, Hui-Min Su, Stefano Salvi, Loïs Monnier, Xinyou Zhu, Xiaoqiang Lv

▶ **To cite this version:**

Zhenpeng Duan, Shao-Yong Jiang, Hui-Min Su, Stefano Salvi, Loïs Monnier, et al.. Beryl as an indicator for elemental behavior during magmatic evolution and metasomatism in the large Shihuiyao Rb-Nb-Ta-Be deposit, Inner Mongolia, NE China. Ore Geology Reviews, 2024, 166, pp.105940. ⟨10.1016/j.oregeorev.2024.105940⟩. ⟨hal-04780286⟩

HAL Id: hal-04780286

https://hal.science/hal-04780286v1

Submitted on 13 Nov 2024

HAL is a multi-disciplinary open access archive for the deposit and dissemination of scientific research documents, whether they are published or not. The documents may come from teaching and research institutions in France or abroad, or from public or private research centers.

L'archive ouverte pluridisciplinaire **HAL**, est destinée au dépôt et à la diffusion de documents scientifiques de niveau recherche, publiés ou non, émanant des établissements d'enseignement et de recherche français ou étrangers, des laboratoires publics ou privés.

HAL Authorization

Ore Geology Reviews 166 (2024) 105940

Contents lists available at ScienceDirect

Ore Geology Reviews

journal homepage: www.elsevier.com/locate/oregeorev

Beryl as an indicator for elemental behavior during magmatic evolution and metasomatism in the large Shihuiyao Rb-Nb-Ta-Be deposit, Inner Mongolia, NE China

Zhenpeng Duan [a,b], Shao-Yong Jiang [a,*], Hui-Min Su [a,*], Stefano Salvi [b], Loïs Monnier [b], Xinyou Zhu [c], Xiaoqiang Lv [c]

[a] State Key Laboratory of Geological Processes and Mineral Resources, Collaborative Innovation Center for Exploration of Strategic Mineral Resources, School of Earth Resources, China University of Geosciences, Wuhan, 430074, PR China
[b] GET, CNRS/IRD/UPS/CNES, Toulouse University, 14 avenue Edouard Belin, 31400 Toulouse, France
[c] Sino-Zijin Resources Ltd., Beijing 100012, PR China

ARTICLE INFO

Keywords:
Beryl
Magmatic evolution
Fluid metasomatism
Fluid exsolution
Shihuiyao deposit

ABSTRACT

In the large Shihuiyao Rb-Nb-Ta-Be deposit, a beryl-bearing granite was identified with three texturally different zones that show an increasing degree of fractionation, including the albite granite (bottom zone), albite granite with pegmatite pockets (intermediate zone), and intercalation of granite and pegmatite layers (top zone). Beryl occurs both in the intermediate and top zones. Microtextural (SEM), Raman spectra, and trace-element (LA-ICP-MS) data on beryl from these zones shed new light on the behavior of trace elements during magmatic-hydrothermal evolution.

In the intermediate zone, magmatic beryl (Brl-1) has a homogeneous texture, while beryl in the top zone (Brl-2) can be divided into magmatic (Brl-2a) and metasomatic subtypes (Brl-2b). The magmatic Brl-2a shows oscillatory zonation, whereas the metasomatic Brl-2b is darker in BSE images and highly porous. Fractional crystallization led to an increase in Na, Sc, Fe, Rb, and Cs contents from Brl-1 to Brl-2a. Comparing these data with those of beryl in other pegmatites worldwide reveals that Cs in beryl is an ideal trace element to monitor the magmatic evolution of the pegmatite host. Distinct textural and chemical features of Brl-2a and Brl-2b reflect metasomatic alteration by a dissolution-reprecipitation process for Brl-2b. In combination with published experimental and fluid inclusion data, we propose that metasomatic fluids exsolved from the magma during late-magmatic stages could transport large amounts of rare metals, such as Ta and Rb. The higher content of Ta in Brl-2b compared to Brl-2a suggests that metasomatic fluids exsolved from the magma play a favorable role in Ta mineralization. In contrast, decreasing Rb contents in Brl-2b is attributed to the high mobility of Rb in the fluid. Such Rb-rich fluids are expected to generate Rb orebodies of economic value surrounding the ore-bearing granite, implying that more investigation into hydrothermal Rb mineralization in the Shihuiyao district is warranted.

1. Introduction

In recent years, rare metals such as Li, Be, Na, Ta, Rb have been treated as strategical critical metals for many countries, which have drawn a lot of attentions in the economic geology society (Jiang et al., 2023). Of these rare metals, Be has been treated as one of the most strategic metals facing shortages in China. Beryl is the most abundant and widespread beryllium-bearing mineral in granitic pegmatites and displays a wide variety of colors as a consequence of trace impurities, such as green emerald (Cr and/or V), blue aquamarine (Fe^{2+}), yellow heliodor (Fe^{3+}), red bixbite (Mn^{3+}), and pink morganite (Mn^{2+}) (Černý, 2002; Lum et al., 2016; Khaleal et al., 2022). The chemical variations observed in beryl could be indicative of host-pegmatite evolution. The fractional trend of beryl towards alkali (Na, Li, and Cs)-rich and Fe-Mg-poor, concluded based on major element analysis, has been well documented in various pegmatites worldwide (e.g., pegmatite in the Greer Lake, Manitoba, Černý and Turnock, 1975; Bikita granitic pegmatite, Zimbabwe, Černý et al., 2003; pegmatite from Namivo, Mozambique,

* Corresponding authors.
E-mail addresses: shyjiang@cug.edu.cn (S.-Y. Jiang), suhm@cug.edu.cn (H.-M. Su).

https://doi.org/10.1016/j.oregeorev.2024.105940
Received 6 October 2023; Received in revised form 4 February 2024; Accepted 5 February 2024
Available online 7 February 2024
0169-1368/© 2024 The Author(s). Published by Elsevier B.V. This is an open access article under the CC BY-NC-ND license (http://creativecommons.org/licenses/by-nc-nd/4.0/).

Neiva and Neiva, 2005; Koktokay #3 pegmatite in Altai, China, Wang et al., 2009; pegmatite in the Bratislava and Bojná massifs, Slovakia, Uher et al., 2010; pegmatite in the Velasco district, Argentina, Sardi and Heimann, 2014). Nevertheless, recent studies on trace elements of beryl have revealed that this general trend may not be universally applicable to all pegmatites (e.g., Lum et al., 2016; Bačík et al., 2021; Pauly et al., 2021; Fan et al., 2022; Suo et al., 2022; Lei et al., 2023), and the reason for this difference remain unclear. Other trace elements of beryl, such as Rb, Zn, Sc, and REE, may be potential indicators for monitoring the evolution of host pegmatites due to their systematic changes with magmatic evolution (Neiva and Neiva, 2005; Sardi and Heimann, 2014; Bačík et al., 2021; Pauly et al., 2021). Moreover, the textures and chemical compositions of beryl can also record multiple stages of metasomatism in pegmatites and give insight into the behavior of trace elements during fluid metasomatism (e.g., Novák and Filip, 2010; Aurisicchio et al., 2012; Michallik et al., 2019).

Our investigation focuses on beryl from the large Shihuiyao Rb-Nb-Ta-Be deposit in Inner Mongolia, Northeastern China, which exhibits several generations from the magmatic to hydrothermal stages. Trace-element compositions and Raman spectra were determined on both magmatic and metasomatic beryls based on the textural zoning pattern obtained by scanning electron microscopy (SEM). We carried out a comparative analysis, incorporating published data, to show the differences in the trends of trace element contents in beryl from different pegmatites during magmatic evolution. Following this, we attempted to investigate the possible factors influencing these trends and to identify specific elements within beryl that could serve as universal indicators of magmatic evolution. Then, by combining the available experimental and fluid inclusion data from the literature, we discuss the mobilization of rare metals (particularly Ta and Rb) during fluid metasomatism.

2. Geological setting

The southern Great Xing'an Range (SGXR) is located in the eastern part of the Central Asian Orogenic Belt (Fig. 1a), the largest Phanerozoic accretionary orogen in the world (e.g., Windley et al., 2007; Safonova et al., 2011). Since the Paleozoic, the SGXR underwent the evolution of the Paleo-Asian Ocean, Mongol-Okhotsk Ocean, and Paleo-Pacific Ocean tectonic systems (Meng, 2003; Wu, F.Y. et al., 2011; Xu et al., 2013). The complex tectonic evolution triggered multiple-stage magmatism and metallogenic events in this region, especially the large-scale magmatism and Sn-Pb-Zn-Ag and rare metal mineralization during the Late Mesozoic. This metallogenic event made the SGXR one of the most important rare metal concentrated regions in China (Jiang et al., 2020). A number of large Sn polymetallic and rare metal deposits have been discovered, including the Baerzhe Zr-Nb-REE deposit (Su et al., 2021), the Shihuiyao Rb-Nb-Ta-Be deposit (Duan et al., 2021), the Tailaihua Nb-Ta deposit, and the Weilasituo Sn-Rb-Li deposit (Jiang et al., 2022).

The Shihuiyao deposit is a typical highly evolved granite type Rb-Nb-Ta-Be deposit, similar to the most evolved rare-metal granites worldwide (e.g., Penouta Sn-Ta-Nb deposit in NW Spain, González et al., 2017; Yichun Nb-Ta deposit in SE China, Wu et al., 2018; Nuweibi Nb-Ta intrusion in Egypt, Moussa et al., 2021; Zhaojinggou Nb-Ta-W-Sn deposit in northern China, Zhang et al., 2023a). The proven reserves of Rb_2O are about 870,000 tons at a grade of 0.17–0.93 wt% (average 0.55 wt%) (Sun et al., 2015), with associated (Nb, Ta)$_2O_5$ reaching about 16.21 Mt at a grade of 0.02 % Nb_2O_5 and 0.015 % Ta_2O_5 (Zhou et al., 2022). Six granitic facies were identified in the mining area: siderophyllite monzogranite (Pluton I), muscovite-albite granite (Pluton II-IV), zinnwaldite granite (Pluton V), and zinnwaldite-amazonite granite (Pluton VI) (Fig, 2a). They were emplaced during the Late Jurassic (ca. 145 Ma) and related to the partial melting of a Neoproterozoic juvenile crust (Duan et al., 2021). The wall rocks are the Permian Linxi Formation composed of black slate, *meta*-sandstone, and limestone. Except for barren Pluton I, the other five plutons contain varying degrees of Rb-Nb-Ta mineralization, with the two largest Nb-Ta orebodies hosted in Pluton III and Pluton IV, respectively (The Inner Mongolia Autonomous Region Bureau of Geology, 1986). These two units (Pluton III and IV) are also the dominant Be-bearing granites. Li-Rb mineraliza tion mainly occurs in Pluton V and VI with zinnwaldite (Li and Rb), orthoclase (Rb), and amazonite (Rb) as the main host minerals.

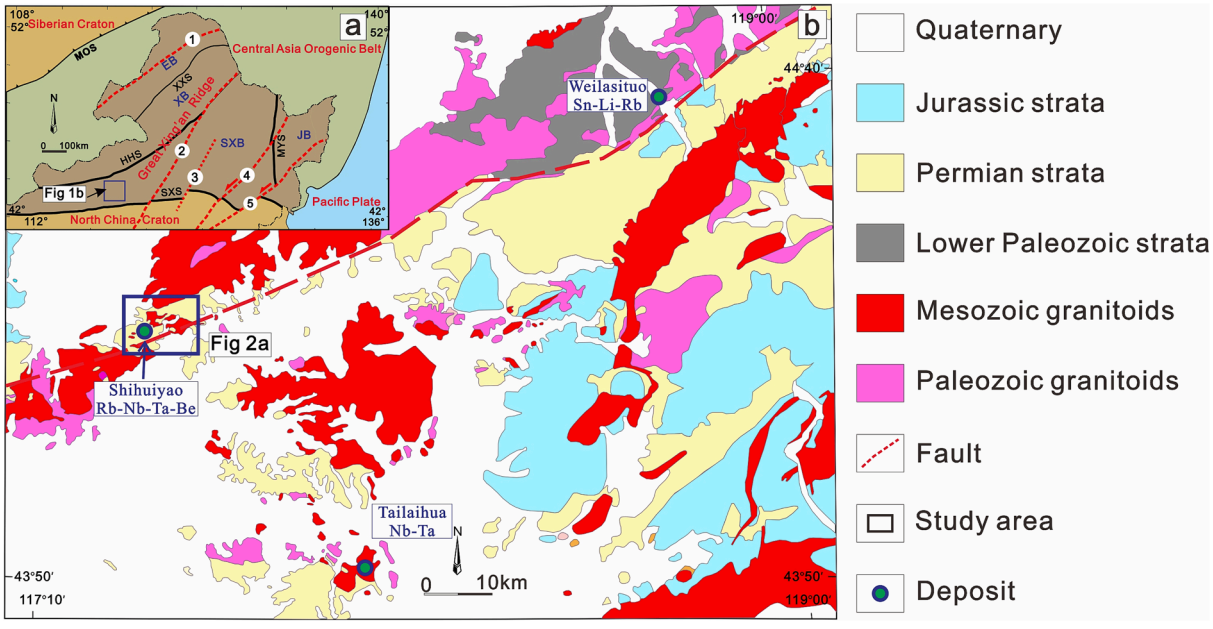

Fig. 1. (a) Tectonic framework of northern China (modified from Duan et al., 2021); EB = Erguna block, XB = Xing'an block, SXB = Songliao-Xilinhot block, JB = Jiamusi block. MOS = Mongol-Okhotsk suture, XXS = Xinlin-Xiguitu suture, HHS = Heihe-Hegenshan suture, MYS = Mudanjiang-Yilan suture, SXS = SolonKer-Xar Moron suture; 1 = Derbugan fault, 2 = Nenjiang-Balihan fault, 3 = Songliao Basin Central fault, 4 = Jiamusi-Yilian fault, 5 = Dunhua-Mishan fault. (b) Regional geological map of the Shihuiyao deposit in the southern Great Xing'an Range (modified from Duan et al., 2021).

3. Beryllium mineralization

In the Shihuiyao area, seventeen Be ore bodies (grading at 0.164–0.314 wt% BeO) were discovered, mainly hosted in Pluton III and IV (The Inner Mongolia Autonomous Region Bureau of Geology, 1986). These Be orebodies occur in greisenized granite, and beryl is the only beryllium-bearing mineral present. We investigated in detail the No. 17 Be orebody, which occurs on the apical parts of Pluton IV (Fig. 2b). This orebody is approximately 3 m thick and 30 m long (The Inner Mongolia Autonomous Region Bureau of Geology, 1986) and particularly well exposed in an exploratory trench at the top of the pluton (Fig. 3). The trench can be divided into three subzones based on petrographic variations, from bottom to top (Fig. 4): granite (bottom zone), granite with pegmatite pockets (intermediate zone), and layered aplite-pegmatite body (top zone).

3.1. Bottom zone

This zone is composed of fine-grained albite granite (Fig. 5a), which consists of quartz (~30 vol%), K-feldspar (~15 vol%), albite (~50 vol %), and muscovite (~5 vol%), with columbite-group minerals (CGM) and monazite as accessory minerals (Fig. 5b-c). This zone has been identified as a Ta orebody (The Inner Mongolia Autonomous Region Bureau of Geology, 1986) (Fig. 3).

3.2. Intermediate zone

This zone is characterized by the development of pegmatite pockets (Fig. 5d-e), which are several centimeters in length and 1–3 cm in width, mainly composed of K-feldspar (~70 vol%), quartz (~30 vol%), and minor albite and muscovite. Only a very few pockets contain beryl. At the scale of the hand specimen, beryl forms short columnar crystals (Brl-1) of light green, about 2 cm long, accompanied by muscovite and minor K-feldspar, quartz, and albite (Fig. 5e-f). Minor CGM with patchy zonation also occurs in this zone and is locally replaced by pyrochlore (Fig. 5g).

3.3. Top zone

The top zone occurs as layered aplite-pegmatite rocks composed of 0.1–1 cm layers of aplite and pegmatite (Fig. 6a-b). The mineral assemblage of the aplite layer is similar to that of the albite granite in the bottom zone, i.e., it consists of albite (~70 vol%), quartz (~20 vol%), K-feldspar (<10 vol%), and minor muscovite (<1 vol%) (Fig. 6c). The pegmatite layer mainly comprises K-feldspar (~70 vol%), quartz (~30 vol%), and minor albite, beryl, muscovite, and cassiterite (Fig. 6a-c). Massive Nb-Ta oxides were observed in the aplite layers, which can be classified into dark CGM and bright pyrochlore (Fig. 6d). CGM exhibits progressive or patchy zonation and is locally enclosed by cracked pyrochlore, which suggests the replacement of CGM by pyrochlore (Fig. 6d). Pegmatite pockets locally occur as 2 cm to tens of centimeter thick bodies in the pegmatite layer and consist of quartz (~50 vol%), beryl (~40 vol%), K-feldspar (~10 vol%), and minor albite and muscovite, with light green beryl (Brl-2) commonly occurring as hexagonal prismatic crystals (1 to 3 cm long) (Fig. 6e-f).

Based on the above observations, beryl only occurs in the intermediate and top zones. Thus, Be mineralization in the Pluton IV mainly occurs in pegmatite.

4. Samples and analytical methods

Samples of the intermediate and top zones were collected from the outcrop exposure. The interior zonation of pegmatite is the key factor in determining the characteristics and evolution stages of associated minerals, including beryl (e.g., Pauly et al., 2021; Fan et al., 2022; Suo et al., 2022). Thus, we divide the beryl in the two subzones into type Brl-1 and type Brl-2. Thin and thick sections were made from these samples for textural and in-situ chemical analyses.

Backscattered electron (BSE) images were obtained using a TESCAN TIMA GMS integrated mineral analyzer equipped with MIRA Schottky Field Emission (FE) Scanning Electron Microscope (SEM) in the Collaborative Innovation Center for Exploration of Strategic Mineral Resources (CIC-ESMR), China University of Geosciences (Wuhan). An acceleration voltage of 25 kV, a beam current of 8nA, and a working distance of ~ 15 mm were used for analysis.

Trace element concentrations of minerals were determined by an NWR 193 HE laser ablation system coupled to an Agilent 7900 single quadrupole ICP mass spectrometer in the CIC-ESMR. Each spot analysis incorporates approximately 30 s of background acquisition followed by 40 s data acquisition from the sample. A spot size of 50 μm was used with a repetition rate of 8 Hz and an energy density of ~ 4 J cm^{-2}. Every 8–10 sample analyses were followed by several analyses of external reference

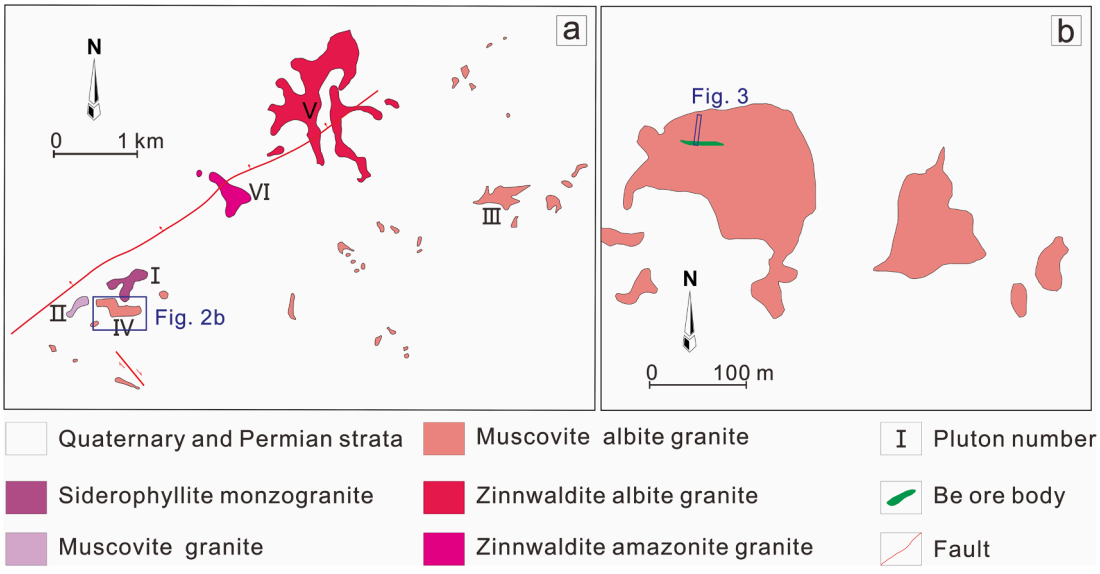

Fig. 2. (a) Geological map of the Shihuiyao deposit (modified from Duan et al., 2021). (b) Geological map of the Pluton IV (modified from The Inner Mongolia Autonomous Region Bureau of Geology, 1986).

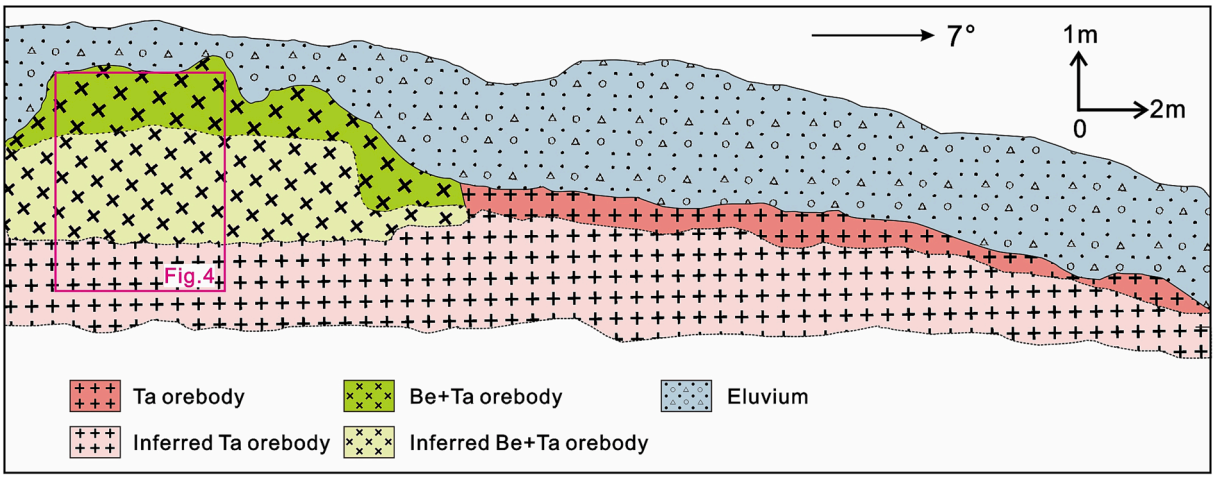

Fig. 3. Schematic cross-section of the exploratory trench on the top of the Pluton IV (modified from The Inner Mongolia Autonomous Region Bureau of Geology, 1986). The inferred orebody was delineated based on the reported thickness of the No. 17 orebody (approximately 3 m).

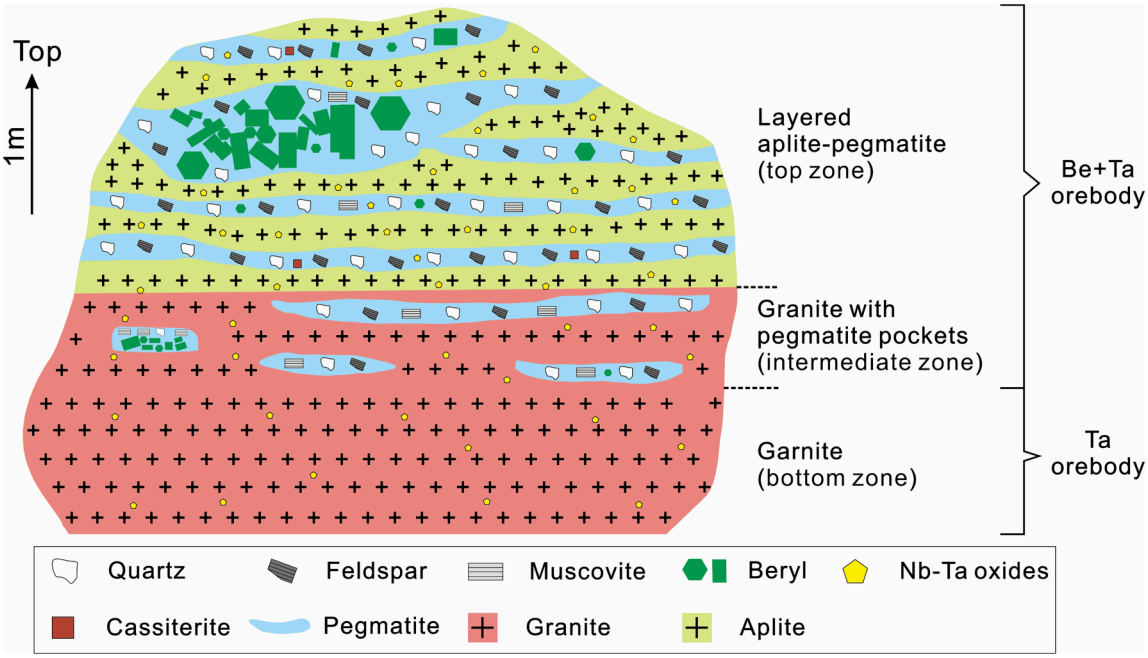

Fig. 4. Schematic diagram of the pegmatite Be orebody.

materials. A total of 35 trace elements, including Li, Be, B, Na, Mg, Al, Si, Sc, Ti, V, Cr, Mn, Fe, Zn, Rb, Zr, Nb, Sn, Cs, La, Ce, Pr, Nd, Sm, Eu, Gd, Tb, Dy, Ho, Er, Tm, Yb, Lu, Hf, Ta were analyzed. NIST SRM 610 was used as quality control (QC) reference material to correct the instrumental time-dependent sensitivity drift, and multiple external standards (NIST 612, BCR-2G, BHVO-2G, and BIR-1G) were selectively used for external calibration. Raw data reduction was performed offline using the ICPMSDataCal software (Liu et al., 2008). The analytical uncertainty is better than 10 % (relative percentage) for most trace elements.

Laser Raman spectra were acquired using a HORIBA Jobin Yvon Odyssey Raman spectrometer in the CIC-ESMR. Raman spectra in the range of 100–1300 cm^{-1} were excited by a green diode laser (532 nm). The output power of the laser was set at 100 mW. All spectra were collected with a 600-grooves/mm grating (defining a spectral resolution of 0.35 ~ 0.65 cm^{-1}) and a 50 × Olympus long working distance objective. The Raman spectrometer was corrected with the signal of silicon at 520.7 cm^{-1} before data collection. Raman and absorption bands were fitted by the Lorentz function with automatic background correction and Savitzky-Golay smoothing.

5. Results

5.1. Beryl textures and chemical compositions

The two types of beryl found in the intermediate and top zones of the pegmatite have distinct textures. Beryl (Brl-1) from the intermediate zone is homogeneous (Fig. 5h), while beryl (Brl-2) in the top zone is systematically zoned, displaying two texturally distinct subtypes (Brl-2a and Brl-2b; Fig. 6g-i). Under the optical microscope, the Brl-2a has a smooth surface, whereas the Brl-2b is very murky (Fig. 6g). In BSE images, Brl-2a shows an oscillatory pattern typical of growth zoning (Fig. 6h-i), while Brl-2b shows darker BSE tones and is characterized by a pitted surface with visible voids (Fig. 6i). In places, the darker Brl-2b surrounds Brl-2a and the boundaries between them are commonly irregular (Fig. 6i). This texture suggests that EDS brighter Brl-2a are relicts, being replaced by the Brl-2b phase.

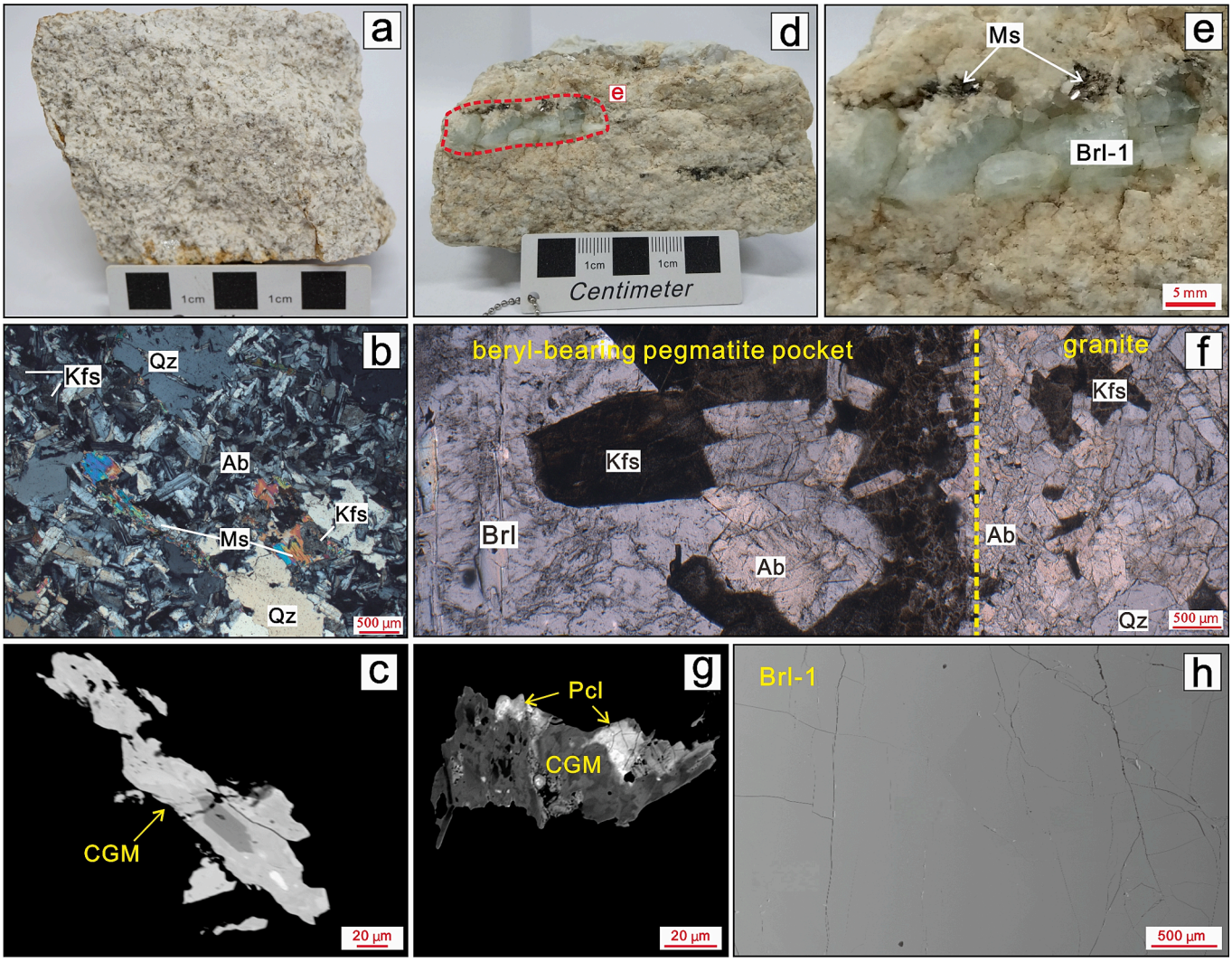

Fig. 5. (a) Photograph of representative hand-specimens of fine-grained albite granite (bottom zone); (b) Representative cross-polarized picture of fine-grained albite granite; (c) Representative backscattered electron (BSE) image of columbite-group minerals in fine-grained albite granite; (d-e) Photograph of representative hand-specimens of the intermediate zone: light green beryl is associated with mica and quartz in the pegmatite pocket; (f) Photomicrograph in cross-polarized light showing the relationship between granite and beryl-bearing pegmatite pocket (intermediate zone); (g) Representative BSE image of columbite-group minerals in the intermediate zone; (h) Representative BSE image of homogeneous beryl from the intermediate zone (Brl-1). **Abbreviation**: Ab = albite; Brl = beryl; CGM = columbite-group minerals; Kfs = K-feldspar; Ms = Muscovite; Qz = quartz; Pcl = pyrochlore. (For interpretation of the references to colour in this figure legend, the reader is referred to the web version of this article.)

The trace element compositions of the different beryl types from the Shihuiyao deposit are listed in Supplementary Table S1. The elements B, Mg, V, Cr, Zr, Nb, and Hf were mostly measured below detection limits and will not be described here. The three types show various chemical compositions consistent with their specific textural features. Brl-1 has lower average contents of Na (1211 ppm), Li (275 ppm), Sc (264 ppm), Fe (1352 ppm), Rb (42.6 ppm), and Cs (344 ppm) than Brl-2a (average 1638 ppm Na, 315 ppm Li, 1210 ppm Sc, 3209 ppm Fe, 88.9 ppm Rb, and 768 ppm Cs) (Table S1; Fig. 7). The Ta contents of Brl-1 and Brl-2a are near the detection limits. There is a distinct compositional boundary between Brl-2a and Brl-2b. Titanium is distinctly enriched in Brl-2b, reaching concentrations up to 100 ppm; in Brl-2a its average is less than 6 ppm (Table S1; Fig. 7). Tantalum also shows a similar enrichment in Brl-2b (average 9.94 ppm) (Table S1; Fig. 7). Other elements, including Na, Fe, and Sc, display a relatively pronounced enrichment in Brl-2b compared to Brl-2a, with average contents increasing from 1572 to 3127 ppm Na, from 3079 to 5521 ppm Fe, and from 1181 to 1410 ppm Sc, respectively (Table S1; Fig. 7). However, Rb and Cs contents in Brl-2b significantly decrease compared to Brl-2a, with average concentrations dropping from 89.7 to 67.8 ppm and from 775 to 520 ppm, respectively (Table S1; Fig. 7). The contents of the rare earth elements in the three types of beryl are extremely low, with most analyses below detection. The total amount of REE is less than 1 ppm (Table S1).

5.2. Raman spectroscopy

The representative Raman spectra of the three types of beryl are shown in Fig. 8, and the Raman active modes and their assignments are listed in Table 1. The Raman bands (Table 1; Fig. 8) were assigned to A_{1g} modes at 320–321, 396, 684, and 1065–1068 cm^{-1}, E_{1g} modes at 526–528 and 1010 cm^{-1} and E_{2g} modes at 445–448 cm^{-1}. Brl-2b lost the 396 cm^{-1} band relative to Brl-1 and Brl-2a (Table 1; Fig. 8). The Raman shifts for the Brl-2a core and Brl-2a rim are consistent.

Brl-1 and Brl-2a have similar Raman spectra (Fig. 8). Two peaks at 320–321 cm^{-1} and 396 cm^{-1} may be caused by the deformation modes of the ring. The peak at 445–447 cm^{-1} may be ascribed to the O-Si-O internal vibration of deformation. The peak at 526–528 cm^{-1} is assigned to Al-O stretching modes. The intense peak at 684 cm^{-1} is characteristic

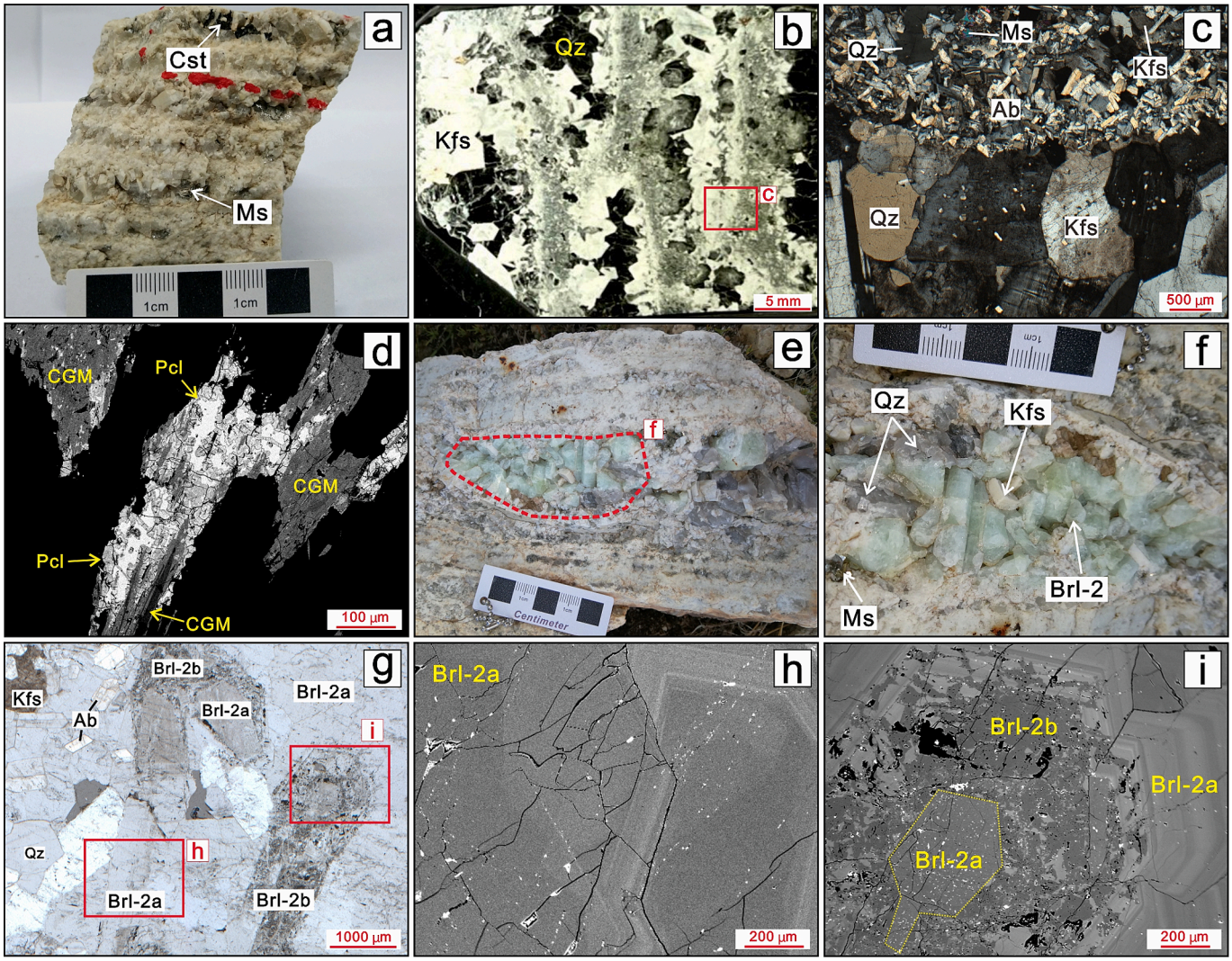

Fig. 6. (a) Photograph of representative hand-specimens of layered aplite-pegmatite rocks (top zone); (b) Photograph of a representative thin section of layered aplite-pegmatite rocks; (c) Photomicrograph in cross-polarized light showing the relationship between granite layer and pegmatite layer; (d) Representative backscattered electron (BSE) image of columbite-group minerals in the aplite layer; (e-f) Photograph of a representative beryl-bearing pegmatite pocket in the pegmatite layer; (g) Photomicrograph in cross-polarized light showing the beryl from the top zone (Brl-2) can be classified into two sub-types: Brl-2a and Brl-2b; (h) Representative BSE image of Brl-2a with oscillatory zonation; (i) Representative BSE image showing dark and porous Brl-2b replacing Brl-2a. The white dots in (h) and (i) are residues of gold coating. **Abbreviation**: Ab = albite; Brl = beryl; Cst = cassiterite; CGM = columbite-group minerals; Kfs = K-feldspar; Ms = muscovite; Qz = quartz; Pcl = pyrochlore.

of the Be-O bond stretching coupled with the ring stretching. The 1010 cm^{-1} band may correspond to the Si-O stretching mode. The intense band at 1065–1068 cm^{-1} may be attributed to Si-O stretching modes.

6. Discussion

6.1. Beryl genesis

Pegmatite pockets, also known as pegmatite segregations, are commonly encountered in highly evolved granites (e.g., London and Kontak, 2012; London, 2014, 2018). They are generally considered to share the same origin as pegmatite dikes, which are the final products of extreme fractionation of a granitic melt (e.g., Jahns and Burnham, 1969; Barnes et al., 2012; Hulsbosch et al., 2014; London, 2018). This is also supported by studies on tourmaline and melt-fluid inclusions found within pegmatite pockets (e.g., Zhao et al., 2019; Yuan et al., 2021). Thus, it can be proposed that Brl-1 from pegmatite pockets in the Shihuiyao deposit has a magmatic origin.

The occurrence of layered pegmatite-aplite bodies has been widely reported in the literature (e.g., London, 2014; Garate-Olave et al., 2017; Wu et al., 2018; Galliski et al., 2020). They are generally interpreted to be related to rapid crystal growth in an undercooled melt (e.g., Webber et al., 1997; London et al., 2012; Breiter et al., 2018). A recent study on cassiterite from different stages of Pluton IV (named Pluton II in Zhang et al., 2023b) in the Shihuiyao deposit has suggested that intercalation of aplite and pegmatite layers (top zone) formed during the magmatic-hydrothermal transition. Additionally, pegmatite pockets in the top zone are distinguished from hydrothermal hollow miarolitic cavities by their solid interiors (Fig. 6e-f). Therefore, we suggest that unaltered Brl-2a is of magmatic origin. In contrast, Brl-2b has the following features (Fig. 6i, 7–8): 1) it still preserves the shape of the primary crystals; 2) it exhibits a sharp compositional boundary with Brl-2a; 3) numerous micro-porosities are present; 4) the absence of a 396 cm^{-1} peak in its Raman spectra implies the breakdown and reconstruction of the beryl crystal structure. All these features reflect that the formation of Brl-2b is related to a dissolution-reprecipitation process (Putnis, 2002). Given the lack of hydrothermal veins in the top zone, we suggest the metasomatic fluid may be the magmatic fluid exsolved from magma during late-

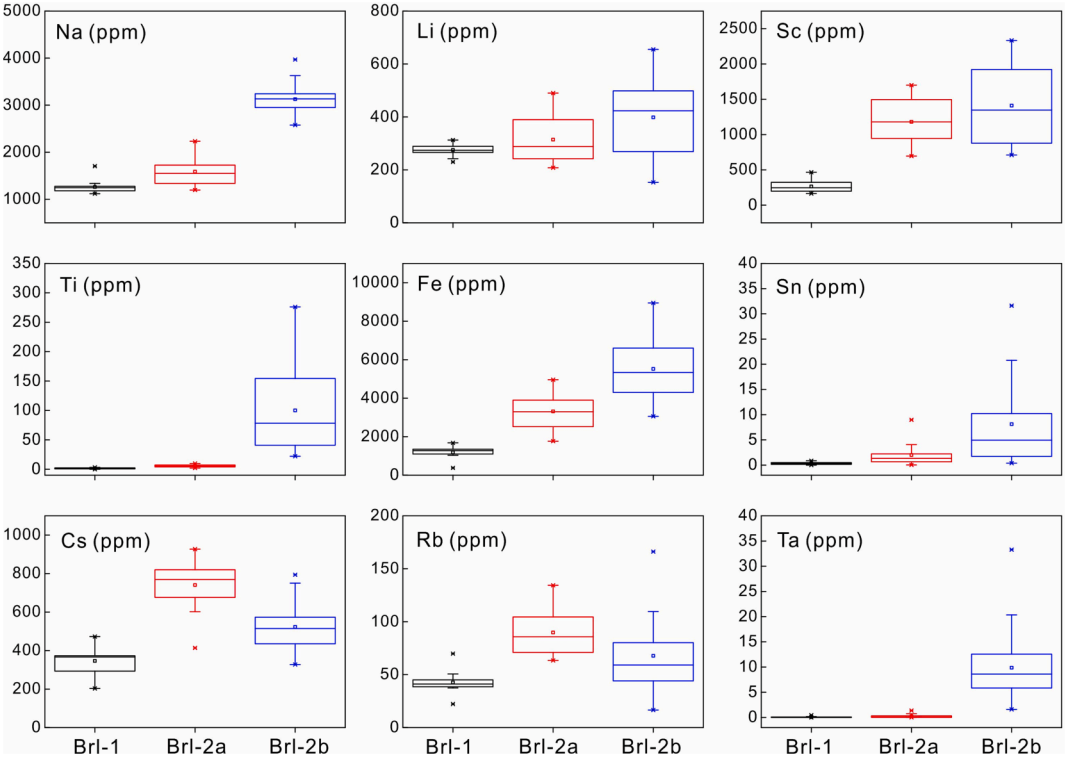

Fig. 7. Box-plot of selected trace element of three types of beryl.

magmatic stages. This fluid shares the same origin as the fluid responsible for the metasomatic caasiterite and quartz-fluorite veins reported by Zhang et al., (2023b). The presence of fluorite within those quartz veins, coupled with the abundant topaz and fluorite in greisen, and the evidence of variations in trace element concentrations in cassiterite, indicates an F-rich nature of the metasomatic fluid (Zhang et al., 2023b).

6.2. *Indicators of magmatic evolution*

In the Shihuiyao deposit, the zonation of the Pluton IV from bottom to top represents the sequence of magmatic evolution, as attested by the increasing concentrations of columbite-group minerals and pegmatitic texture. Thus, we interpret Brl-2a formed from a more evolved melt than Brl-1. Two factors may dominate the chemical variations between Brl-1 and Brl-2a: crystal structure and magmatic evolution.

The incorporation of various elements in beryl is controlled by its crystal structure (e.g., Aurisicchio et al., 1988; Bačík et al., 2021). Two main substitutions in the octahedral and tetrahedral sites control the entry of trace elements into the beryl lattice: (1) octahedral $^{VI}R^{3+}$ (Al^{3+}, V^{3+}, Cr^{3+}, Fe^{3+}, Ti^{4+}) + $^{C}\square \leftrightarrow {}^{VI}R^{2+}$ (Mg^{2+}, Fe^{2+}, Mn^{2+}) + $^{C}R^{+}$ (Na^{+}, K^{+}, Cs^{+}, Rb^{+}) substitution; and (2) tetrahedral $^{IV}Be^{2+}$ + $^{C}\square \leftrightarrow {}^{IV}Li^{+}$ + $^{C}R^{+}$ (Na^{+}, K^{+}, Cs^{+}, Rb^{+}) substitution (Aurisicchio et al., 1988). Based on this, beryl can be further divided into three subtypes (Aurisicchio et al., 1988): normal ($Al_2Be_3Si_6O_{18}$), tetrahedral ($R^{+}Al_2Be_2LiSi_6O_{18}$), and octahedral ($R^{+}AlR^{2+}Be_3Si_6O_{18}$). There is a large compositional gap between tetrahedral and octahedral beryl (Aurisicchio et al., 1988). Binary plots exhibit a positive correlation between R^{2+} and R^{+} in all types of beryl matching the octahedral substitution mechanisms (Fig. 9a), while R^{+} shows no significant correlation to Li (Fig. 9b). Therefore, Brl-1 and Brl-2a should have the same crystal structure, both belonging to octahedral beryl, suggesting that magmatic evolution exerts the primary control on their trace element compositions. That is to say, the compositional variations, along with the correlations between certain elements in beryl from the Shihuiyao deposit, can be used as indicators for the evolution of its host pegmatite.

In general, during magmatic fractionation, late-stage beryl tends to be enriched in alkali elements (e.g., Na, Cs, Li) and depleted in ferromagnesian elements (e.g., Fe, Mg) compared with early-stage beryl (e.g., Černý and Turnock, 1975; Černý, 2002; Černý et al., 2003; Neiva and Neiva, 2005; Uher et al., 2010; Sardi and Heimann, 2014). In particular, the content of Cs in beryl shows a consistent upward trend with magmatic evolution in all pegmatites worldwide (e.g., Černý and Turnock, 1975; Černý, 2002; Neiva and Neiva, 2005; Uher et al., 2010; Sardi and Heimann, 2014; Pauly et al., 2011; Fan et al., 2022; Suo et al., 2022). This trend is also observed in the Shihuiyao deposit, where Cs contents increase from an average of 344 ppm in Brl-1 to an average of 775 ppm in Brl-2a (Fig. 7). In a recent study (Suo et al., 2022), it was observed that Na content of beryl exhibited a declining trend from the wall zone (10,099–15,814 ppm) to the intermediate zone (2262–4041 ppm) inside the Dakalasu No.1 pegmatite (NW China). A similar trend was also noted in the Baishawo deposit (SE China), where Na contents in beryl also decreased from the wall zone (average 0.27 wt%) to the intermediate zone (average 0.22 wt%) (Fan et al., 2022). This declining trend contradicts the increasing Na concentration from Brl-1 (average 1211 ppm) to Brl-2a (average 1572 ppm) in the Shihuiyao deposit (Fig. 7), and is also inconsistent with the documented trend in other pegmatites (e.g., Černý and Turnock, 1975; Černý, 2002; Neiva and Neiva, 2005; Uher et al., 2010; Sardi and Heimann, 2014). The decrease in Na content of beryl from the Baishawo and Dakalasu No.1 pegmatites may be due to the co-crystallization of a large amount of albite (Fan et al., 2022; Suo et al., 2022). There is a slight increase in Li content from Brl-1 to Brl-2a (Fig. 7), whereas, in the scatter plot, only a few data points in Brl-2a are above those in Brl-1 (Fig. 10a). This suggests that Li in beryl from the Shihuiyao deposit may not be a reliable indicator for magmatic evolution. Pauly et al. (2021) reported a gradual decrease of Li content from the core to the rim of a single beryl crystal (Fig. 10a), contrary to the general trend that shows a Li increase in beryl along with magmatic evolution (Černý and Turnock, 1975; Černý, 2002; Neiva and Neiva, 2005; Uher et al., 2010; Sardi and Heimann, 2014; Suo et al., 2022). Although Pauly et al. (2021) did not explain what caused the

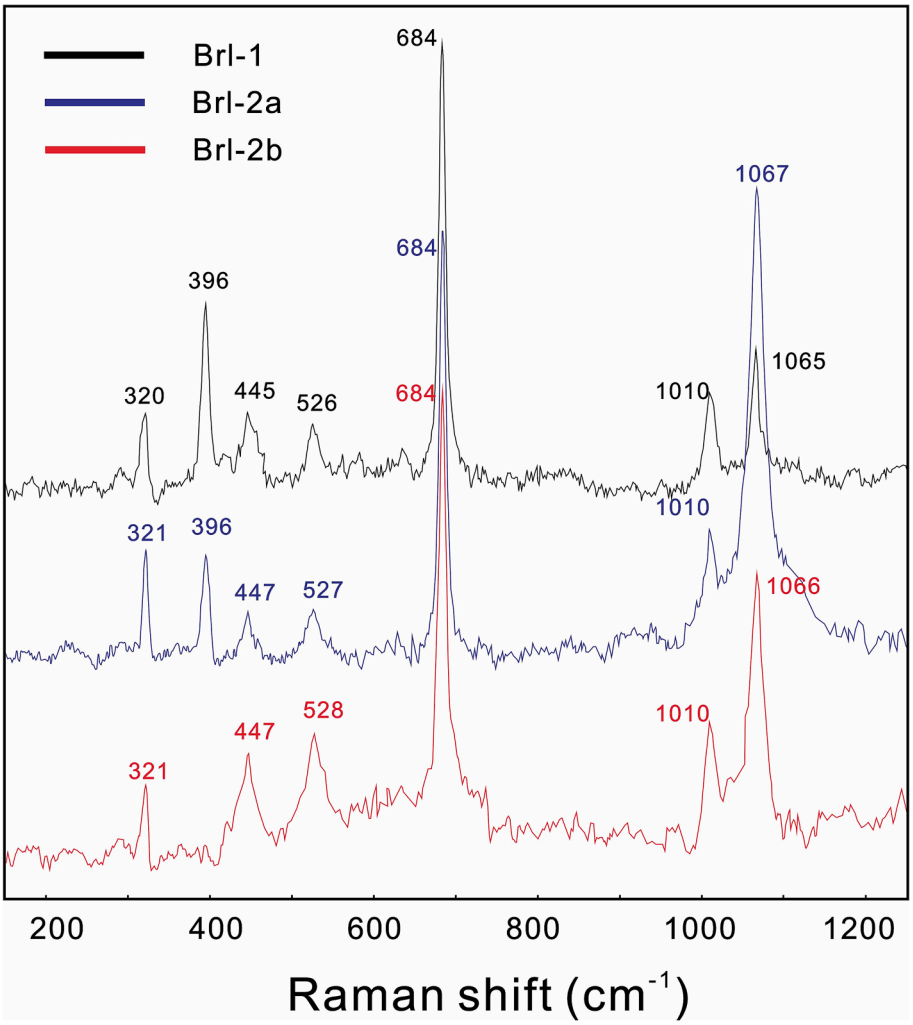

Fig. 8. Representative Raman spectra of three types of beryl.

Table 1
Raman bands (cm^{-1}) and their assignment.

	Assignment	References	Brl-1	Brl-2a	Brl-2b
A_{1g}					
	ring	1,2,3	320	321	321
	ring	1,2,3	396	396	–
	Be-O	1,2,3	684	684	684
	Si-O	1,2,3	1065	1067	1066
E_{1g}					
	Al-O	1,2,3	526	527	528
	Si-O	1,2,3	1010	1010	1010
E_{2g}					
	Si-O	4	445	447	447

References: 1, Adams and Gardner (1974); 2, Hagemann et al. (1990); 3, Charoy et al. (1996); 4, Łodziński et al. (2005);

decreasing Li content of beryl from the core to the rim, they suggested that Li concentration data from beryl may not yield unequivocal interpretations of magmatic evolution. There is a significant increase in Fe from Brl-1 (average 1352 ppm) to Brl-2a (average 3079 ppm). This increase aligns with the core-to-rim trend of a single beryl crystal from the California Blue Mine topaz-beryl pegmatite (Pauly et al., 2021) (Fig. 10b), but is contrary to the fractionation trend observed in other pegmatitic systems (e.g., Neiva and Neiva, 2005; Uher et al., 2010; Suo et al., 2022). Generally, the decreasing Fe content in beryl is due to the co-crystallization of massive Fe-rich minerals, such as tourmaline, garnet, and Nb-Ta oxides (e.g., Neiva and Neiva, 2005; Uher et al., 2010; Suo et al., 2022). In the Shihuiyao deposit, only minor muscovite crystalized in pegmatite pockets (Figs. 5-6). Consequently, the competition for Fe was relatively restricted, leading to a greater incorporation of Fe into Brl-2a. Therefore, the statement that Fe content of beryl decreases with magmatic evolution is questionable, as the influence of competing minerals is an important factor in the variations of Fe content in beryl.

Several other trace elements in beryl can also be used to monitor magmatic evolution, such as Rb, Zn, and Sc (e.g., Sardi and Heimann, 2014; Bačík et al., 2021; Pauly et al., 2021). In the Shihuiyao deposit, the Rb content increases from Brl-1 (average 42.6 ppm) to Brl-2a (average 67.8 ppm), consistent with the evolution trend (Fig. 10c) observed in the beryl from the California Blue Mine topaz-beryl pegmatite (Pauly et al., 2021). Sardi and Heimann (2014) also reported that the extremely low Rb content in beryl reflects the low degree of evolution for its pegmatite host. However, a trend of decreasing Rb content from beryls in the wall zone to the intermediate zone (Fig. 10c) was found in the Dakalasu No.1 Pegmatite, Altai, NW China (Suo et al., 2022). The massive crystallization of megacrystic muscovite in the intermediate zone (Suo et al., 2022) may be responsible for the decreasing trend of Rb content in beryl. Bačík et al. (2021) suggested that beryl with a higher content of Zn may indicate a higher magmatic fractionation degree in its pegmatite host (Fig. 10d), while beryl from the California Blue Mine topaz-beryl pegmatite displayed an opposite trend (Pauly et al., 2021). In the Shihuiyao deposit, Brl-1 and Brl-2a have similar Zn (average 66.4 and 67.1 ppm, respectively) contents (Fig. 10d), indicating that Zn cannot track

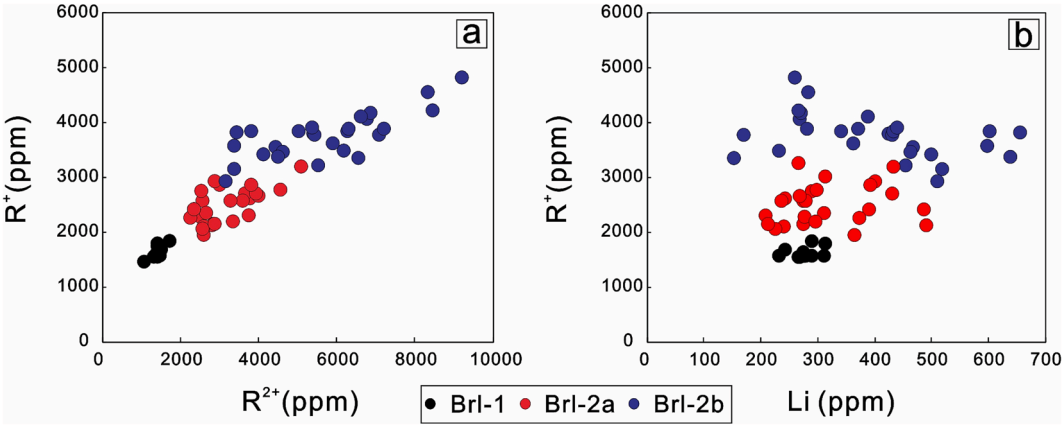

Fig. 9. (a) Coupled substitution of R^{2+} (Fe + Mg + Mn) with R^{+} (Na + Rb + Cs + K). (b) Coupled substitution of Li^{+} with R^{+} (Na + Rb + Cs + K).

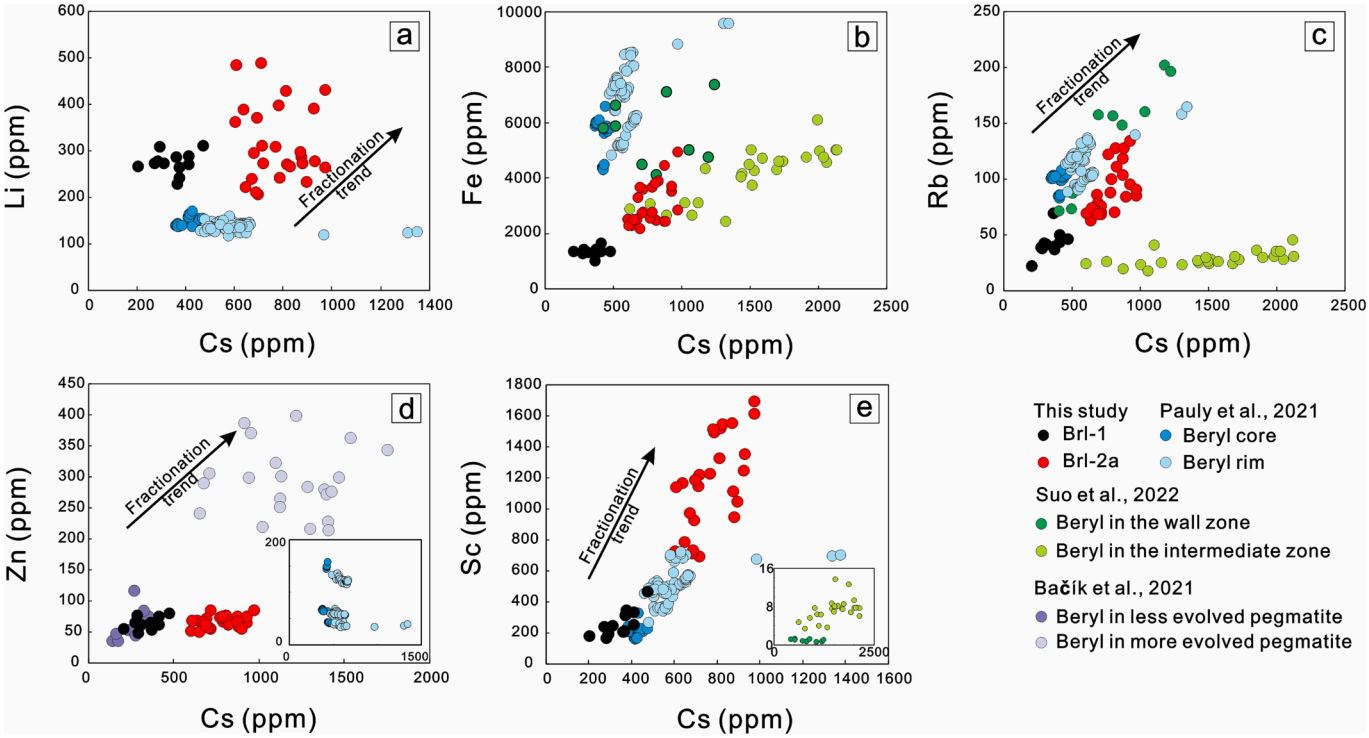

Fig. 10. Diagrams of Li (a), Fe (b), Rb (c), Zn (d), Sc (e) vs. Cs in Brl-1 and Brl-2a.

magmatic evolution. Similarly, no evidence of an increasing Zn content with evolution was found in beryl from the Erongo Volcanic Complex (Lum et al., 2016). It is noteworthy that the structures of Zn-rich and Zn-poor beryls reported by Bačík et al. (2021) are different. This may account for the variations in the Zn content of beryl, as there can be large compositional gaps between beryls of different structures (Aurisicchio et al., 1988). For Sc, a study on four rare metal pegmatites from the Damara Belt in Namibia revealed that beryl formed in a less fractionated environment has higher contents of Sc (Bačík et al., 2021). In contrast, beryl from the California Blue Mine topaz-beryl pegmatite shows an increasing Sc content from the core to the rim (Pauly et al., 2021), consistent with the increase in Sc content from Brl-1 (average 264 ppm) to Brl-2a (average 1181 ppm) in the Shihuiyao deposit (Fig. 10e). A same increasing trend of Sc content in beryl is also observed in the Dakalasu No.1 pegmatite (Fig. 10e) (Suo et al., 2022). This trend agrees with the preference for Sc to enter the F-rich residual melt during magmatic evolution (Shchekina and Gramenitskii, 2008). In the Shihuiyao deposit, the total amount of REE (less than 1 ppm) in beryl is too low to provide reliable information. However, a study of beryl from the granitic pegmatite in Mozambique showed that the total amount of REE increased from the outer zone (1.6–3.7 ppm) to the core zone (4.0–5.8 ppm), which suggests that REE in beryl can indicate the evolution of granitic pegmatite (Neiva and Neiva, 2005). Yet, no such trend was found in beryl from the Velasco Zone of the Pampeana pegmatite province, Argentina (Sardi and Heimann, 2014). These two studies suggested that the concentrations of REE in beryl alone are not a good indicator for magmatic evolution and that more in-depth studies on the behavior of REE in beryl are required.

To sum up, beryl is indeed a useful indicator of magmatic evolution, particularly as its Cs content increases with magmatic evolution, a trend that has been extensively recognized in many pegmatites worldwide (Černý and Turnock, 1975; Černý, 2002; Černý et al., 2003; Neiva and Neiva, 2005; Wang et al., 2009; Uher et al., 2010; Sardi and Heimann, 2014; Bačík et al., 2021; Pauly et al., 2021; Fan et al., 2022; Suo et al., 2022). However, for other elements in beryl, different deposits frequently show different trends due to variations in beryl crystal

structure and mineral paragenesis, and hence render their general application as petrogenetic tools suspect.

6.3. Hydrothermal remobilization

As discussed in Section 6.1, the formation of Brl-2b is related to a dissolution-reprecipitation process that occurred during the interaction of F-rich metasomatic fluids with magmatic Brl-2a. This process can result in a systematic decrease in the content of many trace elements in the reprecipitated phase relative to the primary phase, which has been observed in many natural metasomatic samples (Li and Zhou, 2015; Zeng et al., 2016; Duan et al., 2022). This can explain the lower contents of Rb and Cs in Brl-2b compared to Brl-2a (Fig. 7). Another important feature of the dissolution-reprecipitation process is the addition of some elements with high contents in the reactive fluid into the newly formed phase. This phenomenon has been well documented in the fluorite from the Wujianfang deposit (Duan et al., 2022) where the addition of certain elements significantly elevates their concentration in the reprecipitated fluorite. Therefore, the higher contents of Na, Ti, Fe, Sn, and Ta in Brl-2b reflect the enrichment of these elements in the metasomatic fluids.

One counterargument to the presence of Ta-rich exsolved fluids is that the fluid-melt partition coefficients for Ta are extremely low ($D_{Ta}^{fluid\text{-}melt}$ lower than 0.008; Borodulin et al., 2009). However, it can react with already crystallized Ta-bearing minerals to obtain Ta, as shown by the replacement of CGM with pyrochlore (Fig. 6d). The breakdown of CGM can also release considerable amounts of Ti, Fe, and Sn into the fluid. Two experimental studies have reported that the solubility of Ta in the F-rich fluid is lower than that of Nb (Zaraisky et al., 2010; Timofeev et al., 2017). Therefore, if the metasomatic fluid is simply an F-rich aqueous liquid, it would be expected to exhibit higher contents of Nb than Ta, which would result in a more pronounced increase in Nb content in Brl-2b compared to Ta. However, this is not the case in this study (Nb average 0.26 ppm and Ta average 8.76 ppm in Brl-2b; Table S1). Another candidate is a liquid that contains high concentrations of Na and Si, named by Smirnov et al. (2012) as a hydrosilicate liquid. Such fluids can dissolve high concentrations of Ta over a wide temperature range (up to 600 °C, Smirnov et al., 2012). Hence, it can be inferred that the metasomatic fluid is an F-Na-rich hydrosilicate liquid, which underwent the interaction with magmatic CGM to acquire large amounts of Ta, Ti, Sn, and Fe. This also corresponds to the rise in Na content from Brl-2a (average 1211 ppm) to Brl-2b (average 1572 ppm) (Fig. 7), as well as the high Na contents (about 25,000 ppm) found in fluid inclusions within albite granite of the Shihuiyao deposit (Chen et al., 2023). A similar process has also been proposed for the formation of hydrothermal Ta-rich minerals in the Shangbao, Yichun, and Jianfengling deposits (Wu et al., 2018; Zhao et al., 2021; Diao et al., 2022). Meanwhile, it also suggests that hydrothermal fluids exsolved from magma in the late-magmatic stage may play an active role in the remobilization and enrichment of Ta in highly evolved granitic systems.

It has been experimentally demonstrated that Rb behaves similarly to Ta in the hydrosilicate liquid (Smirnov et al., 2012). In general, the fluid-melt partition coefficients for Rb are low ($D_{Rb}^{fluid\text{-}melt}$ ranging from 0.01 to 0.3; London et al., 1988; Bai and Koster van Groos, 1999; Audetat and Pettke, 2003) and are not affected by melt composition and temperature (Borchert et al., 2010), indicating that Rb preferentially partitions into the melt during fluid exsolution. However, an experimental study conducted by Iveson et al. (2019) has shown that the fluid/melt partition coefficients for Rb can increase with increasing Cl content in the fluid. Additionally, trace element analysis of primary fluid inclusions from the highly evolved topaz granite in Kymi stock (southeastern Finland) also revealed that magmatic fluid exsolved from the magma could contain high concentrations of Rb (650–1050 ppm, Berni et al., 2020), corresponding to extremely high contents of Cl (>1,000,000 ppm, Berni et al., 2020). Chen et al. (2023) reported chemical compositions of fluid inclusions from albite granite of Pluton III and V, as well as greisenized albite granite of Pluton IV. The Cl contents of these fluid inclusions are concentrated between 2 wt% and 4 wt% (Chen et al., 2023). According to Iveson et al. (2019), $D_{Rb}^{fluid\text{-}melt}$ is approximately between 0.13 and 0.4 when the Cl content of fluid is 2–4 wt%. The whole-rock Rb content of Pluton IV averages 910 ppm (Duan et al., 2021). Thus, the maximum Rb concentration in the metasomatic fluids is estimated to be 364 ppm. As mentioned above, the metasomatic fluid is an F-Na-rich hydrosilicate liquid that can transport a large amount of Rb (e.g., Smirnov et al., 2012). Therefore, the Rb content in the metasomatic fluid may be higher than 364 ppm, as evidenced by the highest Rb content in fluid inclusions up to 1296 ppm (Chen et al., 2023). Such a high content of Rb in the fluid can cause the precipitation of Rb into Brl-2b during the dissolution-reprecipitation process, leading to a higher Rb concentration in Brl-2b compared to Brl-2a. Yet, the Rb content in Brl-2b (average 67.8 ppm) is lower than that in Brl-2a (average 89.7 ppm) (Fig. 7). The absence of Rb-bearing mineral inclusions in Brl-2b suggests that Rb exhibits high mobility in F-Na-rich hydrosilicate liquids. These Rb-rich fluids may form hydrothermal Rb orebodies of economic value, like the fluorite-muscovite veins outside Pluton IV observed by Zhang et al., (2023b). Hence, more work on the origin of these hydrothermal veins and the prospecting of hydrothermal Rb mineralization in the Shihuiyao deposit would be of great value.

7. Conclusion

This study conducted textural and in situ trace-element analyses on magmatic and metasomatic beryls from a pegmatitic Be orebody in the Shihuiyao deposit. These data confirm the sensitivity of the Cs content in beryl to the magmatic evolution of its pegmatite host. However, other elements in beryl, such as Na, Fe, Rb, Sc, Zn, and REE, do not seem to be universal tools for monitoring magmatic evolution, as the co-crystallization of associated minerals such as albite, K-feldspar, mica, garnet, Nb-Ta oxides, and tourmaline, as well as the crystal structure of beryl itself, significantly impact the distribution of these elements in beryl. This study also revealed the distinct behaviors of Ta and Rb during fluid metasomatism. Available experimental and fluid inclusion data have demonstrated that the fluid exsolved from magma can transport significant amounts of Ta and Rb. This is evidenced by the notably elevated concentrations of Ta in metasomatic beryl relative to magmatic beryl. However, the decreasing Rb contents in metasomatic beryl can be attributed to the higher mobility of Rb in fluid compared to Ta. These Rb-rich fluids are expected to form hydrothermal Rb orebodies, such as the numerous fluorite-muscovite veins surrounding the ore-bearing granite. Therefore, it is necessary to conduct further studies on the origin of hydrothermal veins and the exploration of hydrothermal Rb mineralization in the Shihuiyao deposit.

CRediT authorship contribution statement

Zhenpeng Duan: Investigation, Formal analysis, Writing – original draft. **Shao-Yong Jiang:** Conceptualization, Methodology, Supervision, Resources, Funding acquisition, Writing – review & editing. **Hui-Min Su:** Methodology, Resources, Writing – review & editing. **Stefano Salvi:** Resources, Supervision, Writing – review & editing. **Loïs Monnier:** Resources, Supervision, Writing – review & editing. **Xinyou Zhu:** Investigation, Resources. **Xiaoqiang Lv:** Investigation, Resources.

Declaration of competing interest

The authors declare that they have no known competing financial interests or personal relationships that could have appeared to influence the work reported in this paper.

Data availability

All data are in the Supplementary Table S1 in this paper

Acknowledgments

We would like to thank Yu-Ying Che, Si-Qi Liu, and Ju-Wei Xiao for their analytical assistance. This study was financially supported by projects from the National Natural Science Foundation of China (No. 92162323, 42321001) and National Key R&D Program of China (No. 2017YFC0602405).

Appendix A. Supplementary data

Supplementary data to this article can be found online at https://doi.org/10.1016/j.oregeorev.2024.105940.

References

Adams, D.M., Gardner, I.R., 1974. Single-crystal vibrational spectra of beryl and dioptase. Journal of the Chemical Society, Dalton Transactions, 1502-1505.
Audetat, A., Pettke, T., 2003. The magmatic-hydrothermal evolution of two barren granites: a melt and fluid inclusion study of the Rito del Medio and Canada Pinabete plutons in northern New Mexico (USA). Geochim. Cosmochim. Acta 67 (1), 97–121.
Aurisicchio, C., Fioravanti, G., Grubessi, O., Zanazzi, P.F., 1988. Reappraisal of the crystal chemistry of beryl. Am. Mineral. 73 (7–8), 826–837.
Aurisicchio, C., Conte, A.M., De Vito, C., Ottolini, L., 2012. Beryl from miarolitic pockets of granitic pegmatites, Elba, Italy: Characterization of crystal chemistry by means of EMP and SIMS analyses. Can. Mineral. 50, 1467–1488.
Bačík, P., Fridrichová, J., Uher, P., Vaculovič, T., Bizovská, V., Škoda, R., Dekan, J., Miglierini, M., Malíčková, I., 2021. Beryl crystal chemistry and trace elements: Indicators of pegmatite development and fractionation (Damara Belt, Namibia). Lithos 404, 106441.
Bai, T.B., Koster van Groos, A.F., 1999. The distribution of Na, K, Rb, Sr, Al, Ge, Cu, W, Mo, La, and Ce between granitic melts and coexisting aqueous fluids. Geochim. Cosmochim. Acta 63 (7/8), 1117–1131.
Barnes, E.M., Weis, D., Groat, L.A., 2012. Significant Li isotope fractionation in geochemically evolved rare element-bearing pegmatites from the Little Nahanni Pegmatite Group, NWT, Canada. Lithos 132–133, 21–36.
Berni, G.V., Wagner, T., Fusswinkel, T., 2020. From a F-rich granite to a NYF pegmatite: magmatic-hydrothermal fluid evolution of the Kymi topaz granite stock. SE Finland. Lithos 364–365, 105538.
Borchert, M., Wilke, M., Schmidt, C., Rickers, K., 2010. Rb and Sr partitioning between haplogranitic melts and aqueous solutions. Geochim. Cosmochim. Acta 74, 1057–1076.
Borodulin, G.P., Chevychelov, V.Y., Zaraisky, G.P., 2009. Experimental study of partitioning of tantalum, niobium, manganese, and fluorine between aqueous fluoride fluid and granitic and alkaline melts. Dokl. Earth Sci. 427, 868–873.
Breiter, K., Durisova, J., Hrstka, T., Korebelova, Z., Vasinova Galiova, M., Müller, A., Simons, B., Shail, R.K., Williamson, B.J., Davies, J.A., 2018. The transition from granite to banded aplite-pegmatite sheet complexes: An example from Megiliggar Rocks, Tregonning topaz granite, Cornwall. Lithos 302–303, 370–388.
Černý, P., 2002. Mineralogy of beryllium in granitic pegmatites. Rev. Mineral. Geochem. 50 (1), 405–444.
Černý, P., Turnock, A., 1975. Beryl from the granitic pegmatites at Greer Lake, Southeastern Manitoba. Can. Mineral. 13, 55–61.
Černý, P., Anderson, A.J., Tomascak, P.B., Chapman, R., 2003. Geochemical and morphological features of beryl from the Bikita granitic pegmatite, Zimbabwe. Can. Mineral. 49, 1003–1011.
Charoy, B., de Donato, P., Barres, O., Pinto-Coelho, C., 1996. Channel occupancy in an alkali-poor beryl from Serra Branca (Goias, Brazil): Spectroscopic characterization. Am. Mineral. 81, 395–403.
Chen, X.K., Zhou, Z.H., Gao, X., Zhao, J.Q., 2023. Insights into the formation of Shihuiyao Ta-Nb deposit in southern Great Xing'an Range, NE China: evidence from chronology and fluid inclusion. Ore Geol. Rev. 158, 105522.
Diao, X., Wu, M.Q., Zhang, D.H., Lu, J.P., 2022. Textural features and chemical evolution of Ta-Nb-W-Sn oxides in the Jianfengling deposit, South China. Ore Geol. Rev. 142, 104690.
Duan, Z.P., Jiang, S.Y., Su, H.M., Zhu, X.Y., Zou, T., Cheng, X.Y., 2021. Geochronological and geochemical investigations of the granites from the giant Shihuiyao Rb-(Nb-Ta-Be-Li) deposit, Inner Mongolia: implications for magma source, magmatic evolution, and rare metal mineralization. Lithos 400–401, 106415.
Duan, Z.P., Jiang, S.Y., Su, H.M., Zhu, X.Y., Jiang, B.B., 2022. Textural features and in situ trace element analysis of fluorite from the Wujianfang fluorite deposit, Inner Mongolia (NE China): insights into fluid metasomatism and ore-forming process. Ore Geol. Rev. 147, 104982.
Fan, Z.W., Xiong, Y.Q., Shao, Y.J., Wen, C.H., 2022. Textural and chemical characteristics of beryl from the Baishawo Be-Li-Nb-Ta pegmatite deposit, Jiangnan Orogen: implication for rare metal pegmatite genesis. Ore Geol. Rev. 149, 105094.
Galliski, M.Á., Martin, R.F., Márquez-Zavalía, M.F., 2020. The Zebra granitic pegmatite, San Luis, Argentina. Can. Mineral. 58, 703–715.
Garate-Olave, I., Müller, A., Roda-Robles, E., Gil-Crespo, P.P., Pesquera, A., 2017. Extreme fractionation in a granite–pegmatite system documented by quartz chemistry: the case study of Tres Arroyos (Central Iberian Zone, Spain). Lithos 286–287, 162–174.
González, L.T., Polonio, G.F., Moro, L.F.J., Fernández, F.A., Contreras, S.J.L., Benito, M. M.C., 2017. Tin-tantalum-niobium mineralization in the Penouta deposit (NW Spain): textural features and mineral chemistry to unravel the genesis and evolution of cassiterite and columbite group minerals in a peraluminous system. Ore Geol. Rev. 81, 79–95.
Hagemann, H., Lucken, A., Bill, H., Gysler-Sanz, J., Stalder, H.A.A., 1990. Polarized Raman spectra of beryl and bazzite. Phys. Chem. Miner. 17, 395–401.
Hulsbosch, N., Hertogen, J., Dewaele, S., Andre, L., Muchez, P., 2014. Alkali metal and rare earth element evolution of rock-forming minerals from the Gatumba area pegmatites (Rwanda): quantitative assessment of crystal-melt fractionation in the regional zonation of pegmatite groups. Geochim. Cosmochim. Acta 132, 349–374.
Iveson, A.A., Webster, J.D., Rowe, M.C., Neill, O.K., 2019. Fluid-melt trace-element partitioning behaviour between evolved melts and aqueous fluids: experimental constraints on the magmatic-hydrothermal transport of metals. Chem. Geol. 516, 18–41.
Jahns, R.H., Burnham, C.W., 1969. Experimental studies of pegmatite genesis: I. a model for the derivation and crystallization of granitic pegmatites. Econ. Geol. 64, 843–864.
Jiang, S.Y., Su, H.M., Xiong, Y.Q., Liu, T., Zhu, K.Y., Zhang, L., 2020. Spatial-temporal distribution, geological characteristics and ore-formation controlling factors of major types of rare metal mineral deposits in China. Acta Geol. Sin. 94 (6), 1757–1773.
Jiang, S.Y., Su, H.M., Zhu, X.Y., Zhu, K.Y., Duan, Z.P., 2022. A new type of Li deposit: hydrothermal crypto-explosive breccia pipe type. J. Earth Sci. 33 (5), 1095–1113.
Jiang, S.Y., Wang, W., Su, H.M., 2023. Super-enrichment mechanisms of strategic critical metal deposits: current understanding and future perspectives. J. Earth Sci. 34 (4), 1295–1298.
Khaleal, F.M., Saleh, G.M., Lasheen, E.S.R., Lentz, D.R., 2022. Occurrences and genesis of emerald and other beryls mineralization in Egypt: a review. Physics and Chemistry of the Earth, Parts a/b/c 128, 103266.
Lei, X.F., Jiang, S.Y., Romer, R.L., Su, H.M., Cao, M.Y., Zhao, C.L., 2023. Petrogenesis of the Weiling beryl-bearing granitic pegmatite – A giant LCT-type pegmatite in the Northern Wuyi area. South China. Ore Geology Reviews 169, 105572.
Li, X.C., Zhou, M.F., 2015. Multiple stages of hydrothermal REE remobilization recorded in fluorapatite in the Paleoproterozoic Yinachang Fe-Cu-(REE) deposit, Southwest China. Geochim. Cosmochim. Acta 166, 53–73.
Liu, Y.S., Hu, Z.C., Gao, S., Günther, D., Xu, J., Gao, C.G., Chen, H.H., 2008. In situ analysis of major and trace elements of anhydrous minerals by LA-ICP-MS without applying an internal standard. Chem. Geol. 257 (1–2), 34–43.
Łodziński, M., Sitarz, M., Stec, K., Kozanecki, M., Fojud, Z., Jurga, S., 2005. ICP, IR, Raman, NMR investigations of beryls from pegmatites of the Sudety Mts. J. Mol. Struct. 744–747, 1005–1015.
London, D., 2014. A petrologic assessment of internal zonation in granitic pegmatite. Lithos 184–187, 74–104.
London, D., 2018. Ore-forming processes within granitic pegmatites. Ore Geology Reviews, 101, 349–383London, D., Hervig, R.L., Morgan, G.B.VI., 1988. Melt-vapor solubilities and elemental partitioning in peraluminous granite-pegmatite systems: experimental results with Macusani glass at 200 MPa. Contrib. Miner. Petrol. 99, 360–373.
London, D., Kontak, D.J., 2012. Granitic pegmatites: scientific wonders and economic bonanzas. Elements 8, 257–261.
London, D., Morgan VI, G.B., Paul, K.A., Guttery, B.M., 2012. Internal evolution of miarolitic granitic pegmatites at the Little Three mine, Ramona, California, USA. Can. Mineral. 50, 1025–1054.
Lum, J.E., Viljoen, F., Cairncross, B., Frei, D., 2016. Mineralogical and geochemical characteristics of beryl (aquamarine) from the Erongo Volcanic complex, Namibia. J. Afr. Earth Sc. 124, 104–125.
Meng, Q.R., 2003. What drove late Mesozoic extension of the northern China-Mongolia tract? Tectonophysics 369, 155–174.
Michallik, R.M., Wagner, T., Rämö, O.T., Heikkilä, P., 2019. The role of magmatic and hydrothermal processes in the formation of miarolitic gem beryl from the Luumäki pegmatite, SE Finland. Eur. J. Mineral. 31, 507–518.
Moussa, H.E., Asimow, P.D., Azer, M.K., Abou El Maaty, M.A., Akarish, A.I.M., Yanni, N. N., Mubarak, H.S., Wilner, M.J., Elsagheer, M.A., 2021. Magmatic and hydrothermal evolution of highly-fractionated rare-metal granites at Gabal Nuweibi, Eastern Desert. Egypt. Lithos 400–401, 106405.
Neiva, A.M.R., Neiva, J.M.C., 2005. Beryl from the granitic pegmatite at Namivo, AltoLigonha, Mozambique. Neues Jahrbuch Für Mineralogie - Abhandlungen 181, 173–182.
Novák, M., Filip, J., 2010. Unusual (Na, Mg)-enriched beryl and its breakdown products (beryl II, bazzite, bavenite) from euxenite-type NYF pegmatite related to the orogenic ultrapotassic Trebic Pluton, Czech Republic. Can. Mineral. 48, 615–628.
Pauly, C., Gysi, A.P., Pfaff, K., Merkel, I., 2021. Beryl as indicator of metasomatic processes in the California Blue Mine topaz-beryl pegmatite and associated miarolitic pockets. Lithos 404–405, 106485.
Putnis, A., 2002. Mineral replacement reactions: from macroscopic observations to microscopic mechanisms. Mineral. Mag. 66, 689–708.
Safonova, I.Y., Seltmann, R., Kröner, A., Gladkochub, D., Schulmann, K., Xiao, W.J., Kim, J.Y., Komiya, T., Sun, M., 2011. A new concept of continental construction in the Central Asian Orogenic Belt. Episodes 34, 186–196.
Sardi, F.G., Heimann, A., 2014. Pegmatitic beryl as indicator of melt evolution: example from the Velasco district, Pampeana pegmatite province, Argentina, and review of worldwide occurrences. Can. Mineral. 52, 809–836.
Shchekina, T.I., Gramenitskii, E.N., 2008. Geochemistry of Sc in the magmatic process: experimental evidence. Geochem. Int. 46 (4), 351–366.

Smirnov, S.Z., Thomas, V.G., Kamenetsky, V.S., Kozmenko, O.A., Large, R.R., 2012. Hydrosilicate liquids in the system Na2O-SiO2-H2O with NaF, NaCl and Ta: evaluation of their role in ore and mineral formation at high T and P. Petrology 20, 271–285.

Su, H.M., Jiang, S.Y., Zhu, X.Y., Duan, Z.P., Huang, X.K., 2021. Magmatic-hydrothermal processes and controls on rare-metal enrichment of the Baerzhe peralkaline granitic pluton, inner Mongolia, northeastern China. Ore Geol. Rev. 131, 103984.

Sun, Y., Wang, R.J., Li, J.K., Zhao, Z., 2015. ^{40}Ar-^{39}Ar dating of the muscovite and regional exploration prospect of Shihuiyao rubidium-multi-metal deposit, Selenhot, Inner Mongolia. Geological Review 61, 463–468 in Chinese with English Abstract.

Suo, Q.Y., Shen, P., Luo, Y.Q., Li, C.H., Feng, H.X., Cao, C., Pan, H.D., Bai, Y.X., 2022. Beryl mineralogy and fluid inclusion constraints on the Be enrichment in the Dakalasu No.1 pegmatite, Altai, NW China. Minerals 12 (450), 1–19.

The Inner Mongolia Autonomous Region Bureau of Geology, 1986. Preliminary geological report on rare metal mining area of Shihuiyao in Xilinhot City. Inner Mongolia Autonomous Region 1–55 in Chinese.

Timofeev, A., Migdisov, A.A., Williams-Jones, A.E., 2017. An experimental study of the solubility and speciation of tantalum in fluoride-bearing aqueous solutions at elevated temperature. Geochim. Cosmochim. Acta 197, 294–304.

Uher, P., Chudík, P., Bačík, P., Vaculovič, T., Galiová, M., 2010. Beryl composition and evolution trends: an example from granitic pegmatites of the beryl-columbite subtype, western Carpathians. Slovakia. Journal of Geosciences 55 (1), 69–80.

Wang, R.C., Che, X.D., Zhang, W.L., Zhang, A.C., Zhang, H., 2009. Geochemical evolution and late re-equilibration of Na-Cs rich beryl from the Koktokay #3 pegmatite (Altai, NW China). Eur. J. Mineral. 21, 795–809.

Webber, K.L., Falster, A.U., Simmons, W.B., Foord, E.E., 1997. The role of diffusion-controlled oscillatory nucleation in the formation of line rock in pegmatite-aplite dikes. J. Petrol. 38, 1777–1791.

Windley, B.F., Alexeiev, D., Xiao, W., Kröner, A., Badarch, G., 2007. Tectonic models for accretion of the Central Asian Orogenic belt. J. Geol. Soc. London 164, 31–47.

Wu, M.Q., Samson, I.M., Zhang, D.H., 2018. Textural features and chemical evolution in Ta-Nb oxides: implications for deuteric rare-metal mineralization in the Yichun granite-marginal pegmatite, southeastern China. Econ. Geol. 113, 937–960.

Wu, F.Y., Sun, D.Y., Ge, W.C., Zhang, Y.B., Grant, M.L., Wilde, S.A., Jahn, B.M., 2011. Geochronology of the Phanerozoic granitoids in northeastern China. J. Asian Earth Sci. 41, 1–30.

Xu, W.L., Pei, F.P., Wang, F., Meng, E., Ji, W.Q., Yang, D.B., Wang, W., 2013. Spatial-temporal relationships of Mesozoic volcanic rocks in NE China: constraints on tectonic overprinting and transformations between multiple tectonic regimes. J. Asian Earth Sci. 74, 167–193.

Yuan, Y.B., Moore, L.R., Mcaleer, R.J., Yuan, S.D., Ouyang, H.G., Belkin, H.E., Mao, J.W., Sublett JR, D.M., Bodnar, R.L., 2021. Formation of miarolitic-class, segregation-type pegmatites in the Taishanmiao batholith, China: the role of pressure fluctuations and volatile exsolution during pegmatite formation in a closed, isochoric system. Am. Mineral. 106, 1559–1573.

Zaraisky, G.P., Korzhinskaya, V., Kotova, N., 2010. Experimental studies of Ta_2O_5 and columbite-tantalite solubility in fluoride solutions from 300 to 550°C and 50 to 100 MPa. Mineral. Petrol. 99, 287–300.

Zeng, L.P., Zhao, X.F., Li, X.C., Hu, H., McFarlane, C., 2016. In situ elemental and isotopic analysis of fluorapatite from the Taocun magnetite-apatite deposit, Eastern China: constraints on fluid metasomatism. Am. Mineral. 101 (11), 2468–2483.

Zhang, T.F., Hou, Z.Q., Pan, X.F., Duan, L.F., Xiang, Z.Q., 2023b. Cassiterite geochemistry and U-Pb geochronology of the Shihuiyao Rb-(Nb-Ta-Be-Sn) deposit, Northeast China: implication for ore-forming processes and mineral exploration. Ore Geol. Rev. 156, 105393.

Zhang, L., Jiang, S.Y., Romer, R.L., Su, H.M., 2023a. Relative importance of magmatic and hydrothermal processes for economic Nb-Ta-W-Sn mineralization in a peraluminous granite system: the Zhaojinggou rare-metal deposit, northern China. Geol. Soc. Am. Bull. 135 (9–10), 2529–2553.

Zhao, Z., Yang, X.Y., Lu, S.M., Lu, Y.Y., Sun, C., Chen, S.S., Zhang, Z.Z., Bute, S.I., Zhao, L.L., 2021. Genesis of Late Cretaceous granite and its related Nb-Ta-W mineralization in Shangbao, Nanling Range: insights from geochemistry of whole-rock and Nb-Ta minerals. Ore Geol. Rev. 131, 103975.

Zhao, H.D., Zhao, K.D., Palmer, M.R., Jiang, S.Y., 2019. In-situ elemental and boron isotopic variations of tourmaline from the Sanfang granite, South China: insights into magmatic-hydrothermal evolution. Chem. Geol. 504, 190–204.

Zhou, Z.H., Breiter, K., Wilde, S.A., Gao, X., Burnham, A.D., Ma, X.H., Zhao, J.Q., 2022. Ta-Nb mineralization in the shallow-level highly-evolved P-poor Shihuiyao granite. Northeast China. Lithos 416–417, 106655.